Anal. Chem. **2002,** *74,* 5169−5174

Entropic Recoil Separation of Long DNA Molecules

Mario Cabodi,* Stephen W. P. Turner,* and Harold G. Craighead

School of Applied and Engineering Physics, Cornell University, Ithaca, New York 14853

A novel technique that can rapidly separate long-strand polymers according to length is presented. The separation mechanism is mediated by a confinement-induced entropic force at the abrupt interface between regions of vastly different configuration entropy. To demonstrate this technique, DNA molecules were partially inserted into a dense array of nanopillars (an entropically unfavorable region) using a pulsed electric field and allowed to relax to their natural state by removal of the field. Molecules of dissimilar lengths (T2 and T7 coliphage DNA) were inserted into this region in such a way that shorter molecules were fully inserted in this region, while longer molecules remained partially across the interface. The longer T2 molecules were observed to recoil entirely out of the pillar array, leaving the shorter T7 molecules inserted, and effecting separation of the two species in a single step. To show how this method can be used for separation of unknown samples, the inserting electric field was pulsed for progressively longer times, allowing passage of progressively longer molecules and producing the equivalent of a conventional electropherogram. The effects limiting resolution in this device are discussed, and the expected separating power of a multistage device is reported. The extracted resolution and running separation time compare favorably with current conventional separation techniques.

Efficient separation of long-stranded DNA molecules remains an important issue in the postgenomic era. Pulsed-field gel electrophoresis (PFGE)[1−3] is still the most commonly used approach for such separations. As with all methods based on sieving by a polymer matrix though, PFGE suffers from problems that result in a decrease in resolution as the DNA gets longer (e.g., irreversible trapping of DNA molecules in the gel fibers[4]). Even though steady-field capillary electrophoresis[5] has been brought forward as a possible alternative to PFGE, it has been recognized[6] that the future of separation science must move away from viscous sieving polymer solutions, and microchip-based technologies have been proposed as the likely tool of choice to tackle this and other problems.[7−11]

Many micro- and nanofabricated devices have been applied to the manipulation and analysis of biological and biochemical samples.[12−17] As well as providing faster analysis times and reduced sample volumes, some of these types of devices have employed completely novel physical effects that are not easily obtained in the macroscopic scale.[18−20] As our ability to decrease the size of useful features in a device improves, different effects can be explored for molecular separation. For instance, when the relevant device dimensions are comparable with the diffusion length scale of a molecule, Brownian ratchets can be used to separate mixtures of molecules with dissimilar diffusion constants.[21−23] When the structure size becomes comparable to or smaller than the size of the molecule, entropic effects tend to dominate the interaction between molecules and the device.[24−27] Recently, one such novel effect was observed in a nanofluidic structure where a new manifestation of entropic force was

* Corresponding authors. E-mail: mc131@cornell.edu. Telephone: 607-255-6286. Fax: 607-255-7658.

(1) Lalande, M.; Noolandi, J.; Turmel, C.; Rousseau, J.; Slater, G. W. *Proc. Natl. Acad. Sci. U.S.A.* **1987**, *84*, 8011−8015.
(2) Slater, G. W.; Noolandi, J.; Rousseau, J.; Turmel, C.; Lalande, M. *Biophys. J.* **1988**, *53*, A475−A475.
(3) Turmel, C.; Brassard, E.; Slater, G. W.; Noolandi, J. *Nucleic Acids Res.* **1990**, *18*, 569−575.
(4) Viovy, J. L.; Miomandre, F.; Miquel, M. C.; Caron, F.; Sor, F. *Electrophoresis* **1992**, *13*, 1−6.
(5) Ueda, M.; Oana, H.; Baba, Y.; Doi, M.; Yoshikawa, K. *Biophys. Chem.* **1998**, *71*, 113−123.
(6) Slater, G. W.; Desrulsseaux, C.; Hubert, S. J.; Mercier, J. F.; Labrie, J.; Boileau, J.; Tessier, F.; Pepin, M. P. *Electrophoresis* **2000**, *21*, 3873−3887.
(7) Abramowitz, S. *Trends Biotechnol.* **1996**, *14*, 397−401.
(8) Colyer, C. L.; Tang, T.; Chiem, N.; Harrison, D. J. *Electrophoresis* **1997**, *18*, 1733−1741.
(9) Burke, D. T.; Burns, M. A.; Mastrangelo, C. *Genet. Res.* **1997**, *7*, 189−197.
(10) Regnier, F. E.; He, B.; Lin, S.; Busse, J. *Trends Biotechnol.* **1999**, *17*, 101−106.
(11) Sanders, G. H. W.; Manz, A. *TrAC, Trends Anal. Chem.* **2000**, *19*, 364−378.
(12) Jacobson, S. C.; Hergenroder, R.; Koutny, L. B.; Ramsey, J. M. *Anal. Chem.* **1994**, *66*, 2369−2373.
(13) Chiem, N.; Harrison, D. J. *Anal. Chem.* **1997**, *69*, 373−378.
(14) Waters, L. C.; Jacobson, S. C.; Kroutchinina, N.; Khandurina, J.; Foote, R. S.; Ramsey, J. M. *Anal. Chem.* **1998**, *70*, 158−162.
(15) Chiem, N. H.; Harrison, D. J. *Clin. Chem.* **1998**, *44*, 591−598.
(16) Li, J. J.; Thibault, P.; Bings, N. H.; Skinner, C. D.; Wang, C.; Colyer, C.; Harrison, J. *Anal. Chem.* **1999**, *71*, 3036−3045.
(17) Wang, J.; Chatrathi, M. P.; Tian, B. M.; Polsky, R. *Anal. Chem.* **2000**, *72*, 2514−2518.
(18) Bakajin, O.; Duke, T. A. J.; Tegenfeldt, J.; Chou, C. F.; Chan, S. S.; Austin, R. H.; Cox, E. C. *Anal. Chem.* **2001**, *73*, 6053−6056.
(19) Berger, M.; Castelino, J.; Huang, R.; Shah, M.; Austin, R. H. *Electrophoresis* **2001**, *22*, 3883−3892.
(20) Brody, J. P.; Yager, P. *Sens. Actuators, A* **1997**, *58*, 13−18.
(21) Duke, T. A. J.; Austin, R. H. *Phys. Rev. Lett.* **1998**, *80*, 1552−1555.
(22) Chou, C. F.; Bakajin, O.; Turner, S. W. P.; Duke, T. A. J.; Chan, S. S.; Cox, E. C.; Craighead, H. G.; Austin, R. H. *Proc. Natl. Acad. Sci. U.S.A.* **1999**, *96*, 13762−13765.
(23) Cabodi, M.; Chen, Y. F.; Turner, S. W. P.; Craighead, H. G. *Electrophoresis*, in press.
(24) Han, J.; Craighead, H. G. *J. Vac. Sci. Technol. A* **1999**, *17*, 2142−2147.
(25) Han, J.; Turner, S. W.; Craighead, H. G. *Phys. Rev. Lett.* **1999**, *83*, 1688−1691.
(26) Han, J.; Craighead, H. G. *Science* **2000**, *288*, 1026−1029.
(27) Han, J. Y.; Craighead, H. G. *Anal. Chem.* **2002**, *74*, 394−401.

10.1021/ac025879a CCC: $22.00
Published on Web 09/12/2002

observed.[28] When a molecule is forced into a confined environment, its free energy increases because of the decrease in the entropy due to the reduced state space of the confined molecule. At an abrupt interface between regions that produce low and high entropy there is an entropic force driven by this free energy change, which tends to push the molecule out of the confined space. A molecule that is either completely in the uniform low-entropy region or in the uniform high-entropy region will experience no force; only molecules that straddle the boundary will be affected. This paper reports how this effect has been exploited to separate molecules according to length.

The first part of this report describes the fabrication process and the setup for the experiments. Details of the molecular biology protocols and microscopy are also given. In the second part, the experimental results are presented and analyzed to obtain the resolution of this single-stage device, from which we extrapolate the resolving power for a multistage device. Finally, improvements to the current devices are proposed and alternative fabrication methods are discussed.

EXPERIMENTAL SECTION

Device Fabrication. The nanofluidic channels were fabricated using a sacrificial layer removal technique described in detail elsewhere,[29] so only a brief outline of the process is given in this section (also see Figure 1). The starting substrates were silicon (100) wafers. Prior to patterning, the wafers were given a coating of 1.0 μm of thermal silicon dioxide to act as an electrical insulation layer, followed by a 190-nm-thick layer of low-stress silicon nitride to act as the floor material. A sacrificial polysilicon layer was applied directly on top of the floor layer. The thickness of this layer determines the height of the fluid gap of the device and ranged from 50 to 500 nm for the devices used in this study. Electron beam resist was then spin-coated on the wafers and exposed using an electron beam lithography tool (Leica Vector-Beam 6). The pattern was transferred to the polysilicon in a multistep reactive ion etch process, after which the samples were coated with silicon nitride again (a 320-nm layer). To remove the polysilicon sacrificial layer, irrigation holes were etched at regular intervals in the silicon nitride top layer, after which tetramethylammonium hydroxide was used to dissolve the polysilicon. After the sacrificial layer was removed, the perforations in the top layer were resealed using a 2.5-μm layer of very-low-temperature oxide. Photolithography was then used to define loading windows at the ends of the devices, and another dry etch process produced loading holes; Figure 2 shows a cross section of a pillared region obtained this way. Finally, polypropylene reservoirs were glued to the device for sample loading.

Samples and Fluorescence Microscopy. Coliphage T2 and T7 DNA (Sigma, St. Louis, MO) were stained with the intercalating dye YOYO-1 (Molecular Probes, Eugene, OR), keeping the dye-to-base pair ratio at 1:10. The final DNA concentration was ~0.1 μg/mL in a buffer containing 450 mM Tris-borate, pH 8.0, 10 mM EDTA (5× TBE, Sigma) with 3% (v/v) β-mercaptoethanol as an antiphotobleaching agent. The individual molecules were observed with an AX70 upright microscope (Olympus America, Melville, NY), illuminated by a 100-W mercury arc lamp and using a 100×/0.8 NA ultralong working distance objective lens (Olympus). An XF100 filter set (Omega Optical, Brattleboro, VT) was used for fluorescence imaging.

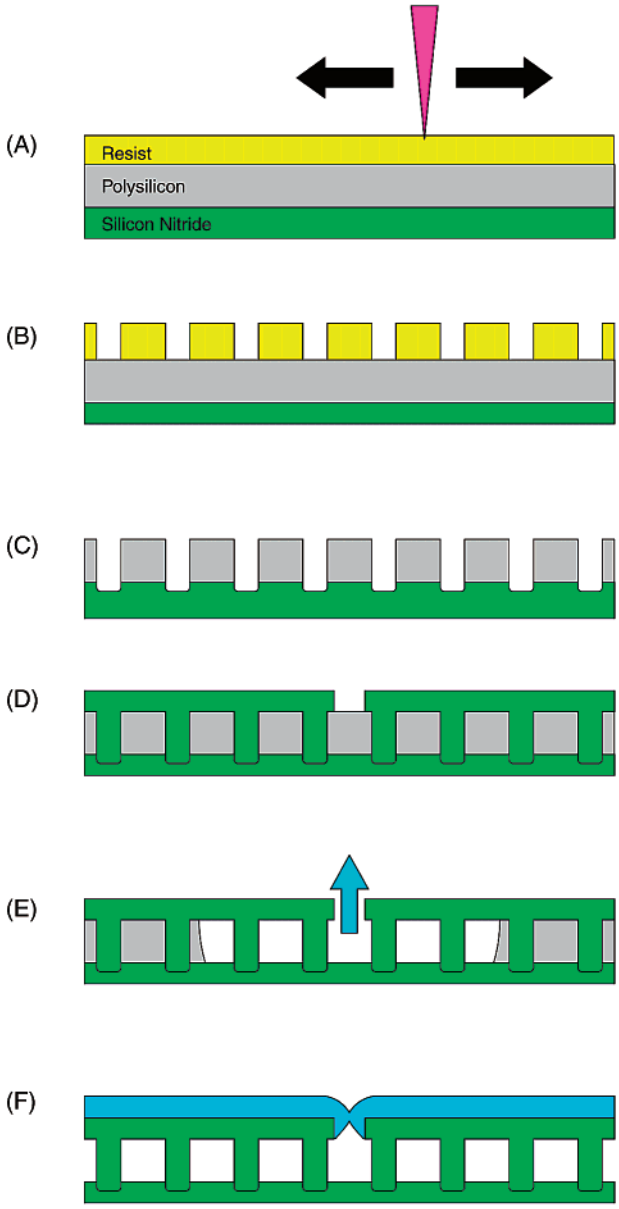

Figure 1. Schematic description of nanofabrication steps. The fabrication begins with the deposition of the silicon nitride floor of the device, followed by the polysilicon sacrificial layer removal. (A) A film of e-beam resist is cast on the surface, and it is exposed with e-beam lithography. (B) The resist film is developed to reveal the latent electron-damage pattern in the film. (C) The pattern is transferred to the polysilicon layer using a reactive ion etch. (D) The polysilicon layer is coated again with nitride. (E) The polysilicon layer is dissolved away through holes in the surface. (F) The holes are resealed with a low-conformality silicon dioxide film.

The microscope was connected to an intensified charge-coupled device camera (Videoscope International, Dulles, VA), and the output was recorded using a digital video processor (DVP32, Instrutech, Port Washington, NY); the images were then analyzed to extract the distribution of molecules. The total molecule count inside a fixed window covering most of the viewing area from the frames (~120 × 80 μm in the actual device) was computed using a counting routine in ImagePro Plus (Media

(28) Turner, S. W. P.; Cabodi, M.; Craighead, H. G. *Phys. Rev. Lett.* **2002**, *88*, (12), 1−4.
(29) Turner, S. W.; Perez, A. M.; Lopez, A.; Craighead, H. G. *J. Vac. Sci. Technol. B* **1998**, *16*, 3835−3840.

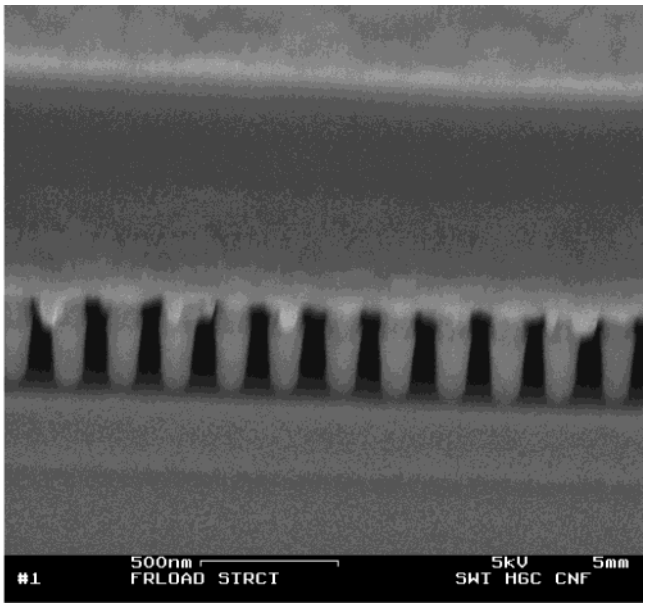

Figure 2. Scanning electron micrograph of a cross section of the finished device. An array of densely spaced nanopillars constitutes the entropically unfavorable region. The pillar spacing was 135 nm and their width ~80 nm.

Cybernetics, Silver Spring, MD). The relative sizes of the two molecules are different enough to allow the software to accurately distinguish between individual T7 and individual T2 molecules. When clusters of molecules were present, the program estimated the number of molecules in each cluster, based on the size of an individual molecule.

Safety Considerations. Nanofabrication of the devices involves extensive cleanroom processing, including chemical and plasma etches and both electron beam and photolithography. All necessary safety precautions should be followed for this processing. The dye YOYO-1 is a possible mutagen, and β-mercaptoethanol is toxic, so gloves should be worn when these chemicals are handled.

RESULTS AND DISCUSSION

Theory. The behavior of the system can be characterized by describing a probability, $P(L,t)$, which quantifies the likelihood that a strand of length L will pass a single barrier after application of a pulse of duration t. For a given strand length, the probability of passage should be zero for sufficiently short pulses, while for sufficiently long pulses, it will tend to unity. If the insertion process were perfect, this probability function would be described by a Heaviside (step) function around the critical pulse duration, t_c. However, at least two effects occur that tend to blur the sharp transition around t_c: *herniation* and *hanging*. If molecules do not initiate penetration from one end, but instead initiate with a single hernia somewhere in the middle, they will be forced out of the favorable region sooner than expected. Thus, herniation can allow molecules to pass through for pulse durations shorter than t_c. The worst case is when the molecule folds exactly in half and inserts at the same critical pulse duration as a molecule half as long inserted at its end. It is worth noting that multiple herniation may complicate the behavior of extremely long molecules in this type of device, since molecules may get stuck in a comblike configuration. This scenario, however, is not likely to occur since the pillar spacing is close in size to the persistence length of double-stranded DNA under these buffer conditions, implying a large energy cost for the formation of hernias. The second effect, hanging, tends to skew the distribution in the other direction: if the molecule initiates from both ends, it may get trapped in the "hanging pulley" conformation, and it will require longer than expected to leave the favorable region. If both ends insert at exactly the same time, they will each proceed a distance of half the chain length and then hang. The time required to escape from such a configuration is discussed by Nixon and Slater,[30] and they arrive at the result that the escape time is proportional to the chain length to first order. For very short pulses, the probability of passage vanishes, and for very long pulses, the probability of passage approaches unity. For intermediate duration, the probability must make a transition from zero to unity around some critical pulse duration, with a characteristic transition width. The exact form of $P(L,t)$ will determine the behavior of the system, so studies are under way to determine this function in more detail.[31] However for the purposes of further analysis here, we assume the transition to be sigmoidal in t and centered around t_c. Since the leading terms in both of the transition-broadening effects described above are linear in strand length, the characteristic width of the probability function is also expected to scale at worst linearly with molecule length. This implies that the minimum strand length difference that allows effective screening by the interface also scales linearly with length. The critical pulse duration, t_c, can be related to the strand length L by the following: $t_c = L/v$, where v is the speed at which the head of the molecule is advancing inside the pillar region. When the head has traveled a distance L inside the pillar region, the molecule will no longer feel the entropic force (this is the definition of the critical insertion time). Using similar structures, it has been shown[32] that the insertion process is entirely local to the portion of the chain at the interface and independent of strand length. Note that there exists a value of applied electric field, defined as the *critical field*, for which entropic and electric forces are exactly balanced, and the molecules experience no center-of-mass motion. This value only affects the initiation of the reptation process into the pillar array. For applied voltages above this critical field, the speed of insertion is then simply given by: $v = \mu_{pillar}E$, where μ_{pillar} is the mobility inside the pillar region and E is the electric field. Combining this with the previous expression yields the following for the critical pulse duration:

$$t_c = L/\mu_{pillar}E \qquad (1)$$

It should be noted that L in this case is the actual elongation of the molecule and not necessarily its full contour length. An estimate of this elongation is given by Turner et al.,[28] ~35% of the contour length in these structures.

If a single pulse of duration t is applied to a population of molecules gathered at the interface, the number of molecules that pass through will be representative of the function $P(L,t)$. However, if a succession of pulses of gradually increasing duration is applied to the *same* population of molecules (assumed to be

(30) Nixon, G. I.; Slater, G. W. *Phys. Rev. E* **1994**, *50*, 5033−5038.
(31) Cabodi, M.; Gaudioso, J.; Turner, S. W. P.; Park, H.; Craighead, H. G., in preparation.
(32) Turner, S. W. P. Ph.D. Thesis, Cornell University, Ithaca, NY, 2000.

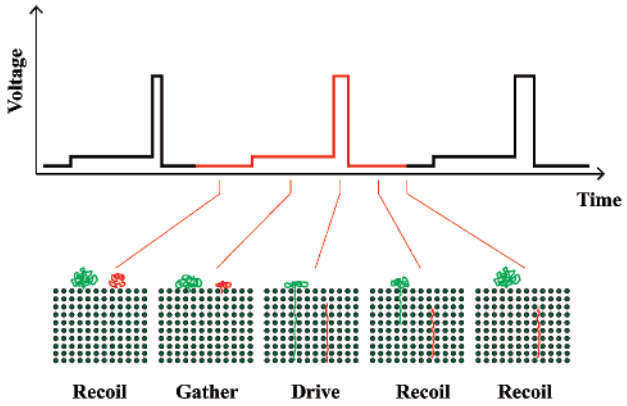

Figure 3. Scheme used for separating molecules of different lengths. During the *gather* phase, molecules are accumulated at the interface with the pillar region. A brief pulse of supercritical voltage (*drive*) inserts shorter molecules fully but longer molecules only partially. During the *recoil* phase, molecules still straddling the interface are completely extracted from the pillar region, while molecules that are fully inserted experience no center-of-mass motion. The *drive* time can be progressively increased to allow passage of progressively longer molecules. The values of pulse durations and voltages used in the experiment are described in the Multistep Separation section.

finite), the resulting distribution of molecules passing the interface will be affected by a combination of the increasing passage probability and the decreasing number of remaining molecules. The early, short pulses will pass few molecules due to insufficient duration. As the pulse duration increases, the rate of passage of molecules increases, peaks, and then decreases again to zero due to depletion of the population. The depletion effect causes this peak to shift to the left of the critical pulse duration, but the peak width still reflects the sharpness of the transition. This effect is discussed further in the section Multistep Separation.

Single-Step Separation. To demonstrate separation, DNA molecules of dissimilar length (T2 and T7 coliphage DNA, 167 and 39 kbp, respectively) were accumulated at the interface with the dense pillar region and separated in a single voltage cycle. The separation process is composed of three steps: a *gather* phase, a *drive* phase and a *recoil* phase. Figure 3 illustrates the function of the three steps. The *gather* uses a subcritical field (below the value required for insertion in the pillar region) to push the population of DNA molecules in the region before the dense pillar region against the boundary; molecules cannot enter the pillar region at this field strength. The *drive* is a short pulse of high field (well over the critical value), which forces the molecules into the dense pillar region; due to the presence of the obstacles, the molecules must reptate into the array (the radii of gyration for T7 and T2 molecules are 1.1 and 2.3 μm respectively, compared to a pillar spacing of ~100 nm). Eventually, some of the molecules will have completely entered the dense pillar region, while others will have some portion still in the free region. The *recoil* phase is the step during which the molecules are separated according to size. If a molecule is not completely in the dense pillar region, it will extract itself due to the entropic force, while molecules that have no part left in the free region will remain stationary.

In the experiment, a voltage pulse exceeding the critical value (~5 V/cm) was applied for ~2 s, which fully inserted the shorter T7 molecules but left the longer T2 molecules generally straddling the interface. Upon removal of the field, molecules crossing the boundary between the two regions were observed to completely recoil out of the pillar region, while the fully inserted molecules experienced no center-of-mass motion. Figure 4 shows the DNA molecules before (a) and after (b) the voltage pulse and recoil. Two clearly visible bands are present at the end of the pulse (a video clip of this single-step separation process is available in the Supporting Information to this report). For a given electric field, the pulse duration needed for complete insertion will correlate with molecule size, shorter molecules advancing while longer molecules are held back. The above procedure can be repeated with the same conditions to maximize the sensitivity between these two particular lengths, or if it is desirable to separate many fractions, the drive pulse duration can be progressively increased to allow passage of progressively longer molecules.

Multistep Separation. To demonstrate how this technique would work with an unknown mixture, a multipulse experiment was devised, in which the duration of the voltage pulse was progressively increased to look at a broad range of lengths (see Figure 5). The mixture of DNA molecules was gathered at the abrupt interface using a subthreshold electric field (0.25 V/cm) for 15 s. Drive pulses of 5 V/cm were applied with durations starting at 0.1 s, growing longer with each successive pulse to a final duration of 6 s, in 0.01-s increments. After each pulse, an interval of zero applied field was allowed for the molecules to recoil, starting at 15 s, and increasing to a duration of 65 s in 0.1-s increments to allow sufficient time for the longest molecules to recoil. Both drive and recoil times were increased linearly. The total running time for this experiment was determined by the total number of pulses and was ~9 h. It should be noted that this time could be reduced significantly by choosing a larger pulse duration

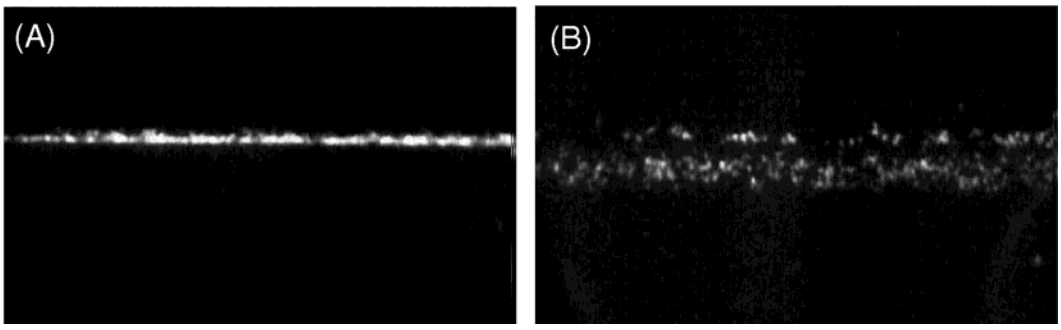

Figure 4. Single-step separation of T2 and T7 DNA molecules. Using a voltage pulse of ~2 s, the shorter T7 molecules were fully inserted, while the longer T2 molecules remained partially in the entropically favorable region. When the field was removed, the longer molecules extracted themselves from the pillar region. Note that the T7 molecules were present in excess for this experiment. A video clip of this process is available with the Supporting Information to this report. (Note: the frame rate in the video clip was increased to 30 frames/s).

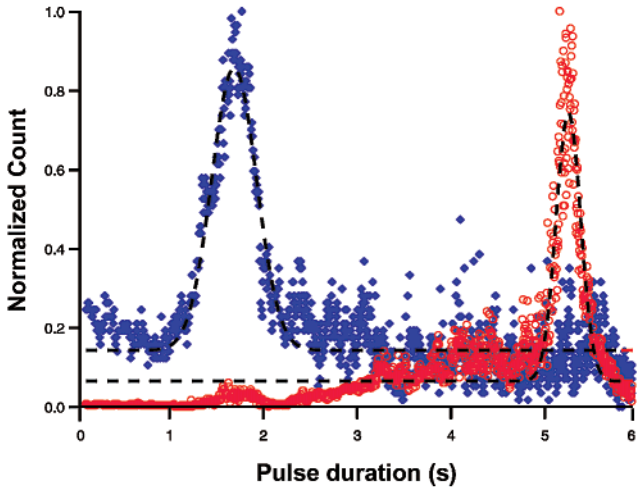

Figure 5. Normalized molecule count vs drive pulse duration for a multistep separation. The blue diamonds correspond to the T7 molecules, and the red circles correspond to the T2 molecules. The molecules were counted using an automated counting routine in ImagePro Plus. Three size "bins" were used, corresponding to individual T7 molecules, individual T2 molecules, and clusters of T2 molecules. The program counted the number of individual molecules and estimated the number of molecules in the clusters. Both distributions were fitted to Gaussian distributions (the values of χ^2 for the two fits were 6.14 and 5.12, respectively).

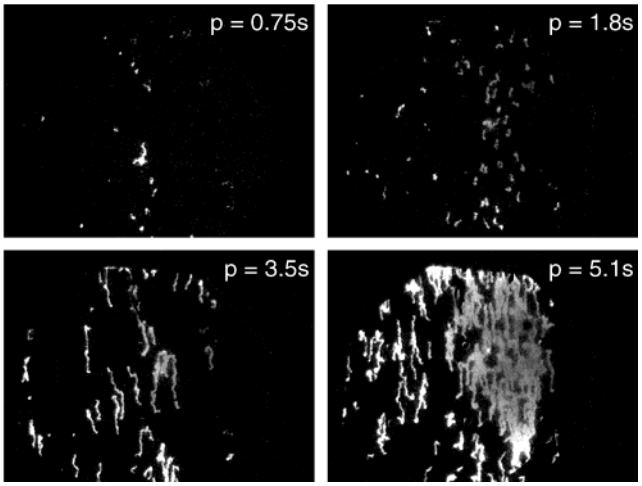

Figure 6. Individual frames extracted from the videos of a single-stage, multistep separation. The progression of frames (taken at drive pulse durations t = 0.75, 1.8, 3.5, and 5.1 s, respectively) shows that as the pulse duration is increased, progressively longer molecules make it past the entropically unfavorable region. At first, only the shorter T7 molecules, and then the longer T2 molecules are observed, confirming that the device is separating the species according to length. The applied field was 5 V/cm, a value exceeding the required insertion voltage.

increment or a higher drive voltage (see Discussion section). The observation volume was positioned to view the contents of the device downstream ($\sim$ 40 μm) from the abrupt interface and record the passage of molecules that penetrate fully into the unfavorable region.

DISCUSSION

The number of molecules passing the abrupt interface as a function of pulse duration is shown in Figure 5 (molecules were identified on the basis of total fluorescent intensity and counted); since differing relative amounts of T2 and T7 molecules were used, a normalized count is shown here. Two distinct peaks are clearly visible corresponding to the two DNA types present in the mixture. A direct examination of frames taken from the video (see Figure 6) confirms that these peaks correspond to the different DNA species and that the device is indeed separating the molecules according to length. The peaks were fitted to two Gaussian distributions, centered at $t_{T7} = 1.689 \pm 0.004$ s, and $t_{T2} = 5.251 \pm 0.002$ s respectively; the characteristic widths are $\sigma_{T7} = 0.337 \pm 0.006$ s and $\sigma_{T2} = 0.184 \pm 0.003$ s. It is worth noting that σ_{T2} is smaller than σ_{T7}, suggesting that the scaling of the resolution with length is better than expected.

While it may seem appropriate at first to identify the center of each peak with the corresponding critical pulse duration for each species, this is not the case. Since the population of molecules at the interface is finite (i.e., does not get replenished between pulses), each new pulse is applied only to the fraction of molecules remaining from the previous pulses. The observed distributions of molecules are in fact the product of the probability of passage, $P(L,t)$, and the instantaneous number of molecules at the interface, $N(t)$. The position of each peak was thus shifted to the left, depending on the number of previously applied pulses.

It should be noted that some smaller molecules are still detected for long pulse durations; however, their number is very small. A fraction of these are likely to be latecomers to the separation region. The devices used in these studies lacked a sophisticated loading system and so stray material from distant regions of the device created some of this undesirable background. Another fraction can be attributed to photocleavage of the longer T2 molecules. Irreversible binding of T7 DNA to the pillar array was not observed to a degree that could cause such a tail in the distribution.

Neither the latecomers nor photocleavage of longer molecules will affect the resolving power of the system. The latecomers can be eliminated through the use of a three-terminal or four-terminal loading strategy, and the photocleavage can be eliminated by avoiding illumination of the system until after separation. At worst, these effects produce a background as seen in Figure 5.

The resolution of separation can be extracted from the positions and widths of the two peaks. Using the fact that two bands are resolved when their peaks are separated by $\Delta t = [\sigma_i + \sigma_{i+1}]$; the resolution of separation is then given by $R_s = \Delta t/2[\sigma_{T2} + \sigma_{T7}] = 3.4$. The coefficients of variation for the two peaks ($CV_i = \sigma_i/t_i$) are $CV_{T7} = 0.199$ and $CV_{T2} = 0.035$. Assuming that a resolution equal to 0.5 is required for minimally resolved peaks, the value for R_s achieved here implies that almost seven bands could be resolved between the T7 and T2 peaks. Assuming linear resolution in this size range, a hypothetical peak at $\sim$148 kbp could then be resolved from the 167-kpb peak, corresponding to a percentage resolution of $\sim$11%.

Predicted Performance of Multistage Separation and Suggested Improvements on the Design. To enhance the resolution of the system, many similar interfaces could be serially combined. If the DNA molecules are undamaged by the application of a pulse, it is reasonable to assume that the passage or failure to pass a given stage will have no effect on the probability of passage at the next stage or in a second attempt at the same gate. Under these circumstances, the resolution of a multistage system is can be computed using binomial statistics. If strands of

length L_i are placed in a device with M stages with period d, the average positions after N pulses for the molecules are $dNP(L_i,t)$, respectively. Note that even after the fractions are completely separated, each fraction will occupy several stages of the system. For large values of N, the molecules will be distributed in bins, corresponding to the stages of the device, around the average position according to the binomial distribution, and the width of each distribution will be $\sigma_i = d(NP(L_i,t)(1 - P(L_i,t)))^{1/2}$, where σ_i is the width of the distribution for the ith strand length. As mentioned earlier, the exact details of $P(L,t)$ will be needed to determine the final distribution of molecules after passing through M gates, but for a large number of gates, the distribution will be dominated by binomial statistics. To illustrate the dependence of the resolution on the number of stages, we consider the case of DNA fragments of a known length (as in the single-step experiment reported above) in a device with a fixed number of stages operated with a fixed pulse duration. Then the expected separation between two peaks is approximately given by $\Delta x \approx dN(P(L_i,t) - P(L_{i-1},t)) \propto N$, and the width of the peaks scales with $\sigma \propto \sqrt{N}$; the resolution will thus improve with the square root of the number of applied pulses. To determine how the resolution scales with the number of gates, we note that the position of the farthest peak after N pulses is approximately $dMP(L_i,t)$. Thus $M \propto N$, and the resolution should also improve with the square root of the number gates. Combining this with the measured resolution for a single stage, only 100 stages would be needed for the coefficient of variation to be ~0.3−2% or a ~1.1% resolution.

This is significant for two reasons: first, this level of resolution would surpass what is currently achieved by other methods; second, if 30 s is allowed for each pulse sequence (a reasonable value for this range of DNA lengths, attainable, for example, by increasing the applied voltage), the whole process could take place in under 1 h. It should be noted that each stage of separation in this device uses an area only 90 μm wide (as in the devices used here) and a length long enough to accommodate the longest strand of interest. For fully stretched T2 DNA, this is only 50.8 μm. This means that the entire separation could take place in a structure 90 μm wide and ~5 mm long.

Another important factor to be considered is the total recoil time. Even though the mechanism of entropic recoil separation should have no intrinsic upper limit of the resolution, there is a rate-limiting effect that makes the method impractical for very long molecules. Since the recoil force is constant, longer molecules require more time to recoil from the dense pillar region; the recoil time scales with the square of the length (longer molecules have greater friction and they have farther to go). The application of high-frequency longitudinal or lateral ac fields could accelerate the rate of recoil: the shaking motion induced by an ac field has the same effect as increasing the temperature of the molecule, thus increasing the change in free energy due to its movement. Because the recoil time depends on the square of the length, eventually all of these methods will become unreasonably slow as the strand length increases.

CONCLUSIONS

The entropic recoil separation differs from conventional separation techniques in that it effects a direct measurement of the contour length of the molecule while other methods infer the length from indirect measurements, usually electrophoretic mobility. These other methods suffer from a rapid decrease in the intrinsic resolution as molecules get larger. The separation technique presented here is expected not to exhibit the same adverse length dependence and could in principle separate DNA molecules over a wide range of lengths with unprecedented resolution.

The entropic recoil separation strategy holds good potential as an alternative to conventional sieving techniques for long DNA and biopolymer separation. The relative ease and flexibility of the fabrication process used here implies that a variety of different parameters could be explored to optimize separation performance. At the same time, a better theoretical understanding of the process itself, including the exact form of the passage probability function, will be a precious aid in the design of future devices. Possible improvements include measures that minimize the effect of herniation and hanging, making the transition around the critical pulse duration much sharper and increasing the intrinsic resolution. Once the optimal design for a single-stage device has been found, it will be straightforward to stage many of these "entropic gates" to maximize the overall resolving power.

The tests here were done in a nanofabricated fluidic structure, since the two-dimensional structure of the nanofluidic device is ideal for examination of the DNA molecules as they traverse the onset of the constricted region. The abrupt onset of the low-entropy region required for the entropic recoil separation technique to function could in principle be constructed by a number of other means. It would be plausible to use mesoporous materials such as zeolites,[33] block copolymer matrixes,[34,35] or block copolymer−ceramic hybrids.[36] Nucleopore membranes[37,38] have sufficiently small and dense pores to function in entropic recoil separation as well. These materials are certainly of interest for future implementations of this method.[31] Finally, it should be noted that while the entropic recoil separation was demonstrated here with DNA molecules, this separation method could be used with any polymer, so long as a suitable entropically unfavorable region can be constructed: in the case of proteins, for example, this could be achieved with mesoporous materials.

ACKNOWLEDGMENT

This work was supported by the NIH Grant HG01506. This work was performed in part at the Cornell Nanofabrication Facility (a member of the National Nanofabrication Users Network), which is supported by the National Science Foundation under Grant ECS-9731293, its users, Cornell University and Industrial Affiliates.

SUPPORTING INFORMATION AVAILABLE

Video sequence of one-step separation (.avi format). This material is available free of charge via the Internet at http://pubs.acs.org.

Received for review June 21, 2002. Accepted August 30, 2002.

AC025879A

(33) Meyer, W. M.; Olson, D. H. *Atlas of zeolite structure types*, 2nd ed.; ed.; Butterworth: London, 1988.
(34) Mansky, P.; Chaikin, P.; Thomas, E. L. *J. Mater. Sci.* **1995**, *30*, 1987−1992.
(35) Harrison, C.; Park, M.; Chaikin, P.; Register, R. A.; Adamson, D. H.; Yao, N. *Macromolecules* **1998**, *31*, 2185−2189.
(36) Simon, P. F. W.; Ulrich, R.; Spiess, H. W.; Wiesner, U. *Chem. Mater.* **2001**, *13*, 3464−3486.
(37) Beck, R. E.; Schultz, J. S. *Science* **1970**, *170*, 1302.
(38) Beck, R. E.; Schultz, J. S. *Biochim. Biophy. Acta* **1972**, *255*, 273.